RESEARCH ARTICLES

# A signal-strength model for gravity-field spectrum components in a local space

Liu Hongwei[1,*], Wang Zhaokui[2], Zhang Yulin[1,2]

[1] Institute of Aerospace Science and Engineering, National University of Defence Technology, Changsha, China

[2] School of Aerospace, Tsinghua University, Beijing, China

## ABSTRACT

*In the Earth gravity-field model, potential coefficients are projections of the Earth gravitational potential on the corresponding spherical harmonics by degree and order. These coefficients reflect the spectral composition of the Earth gravitational potential in the whole space, but they cannot reflect the spectral composition in a local area. In this study, the Earth gravitational potential was projected on spherical harmonics in a local area using a window function introduced to facilitate the mathematical expressions. Then a model for the spectral structure of the Earth gravitational potential in the local area was established. The model can reflect the signal strength of any gravity-field spectrum component in the local area, which adds information for the description of the gravity field of the Earth, and which has great significance for Earth-sciences research and satellite gravity measurements. Taking the third-degree coefficients, for example, the signal-strength distributions of potential coefficients were computed. The data show that the signal-strength distributions of third-degree coefficients on the sphere surface are independent of the longitude. Among the third-degree coefficients, the zero-order, first-order and second-order coefficients are stronger near the two poles of the Earth, while the third-order coefficient is stronger near the equator.*

## 1. Introduction

The Earth gravity field is one of basic physical fields of the Earth, and it reflects information relating to matter distribution inside the Earth and affects physical events on the Earth and in the neighboring space. Therefore, research into the Earth gravity field is always a hot issue in geodesy [Jinsheng 2001, 2002]. The gravity field outside the Earth is caused by matter inside the Earth. As well as the shape of the Earth affecting the Earth gravity potential, this is also affected by the asymmetry of the matter density distribution inside the Earth [Jian 1994]. Researches into the Earth shape and density are two basic missions in Earth gravity research [Xiaoguang et al. 2000]. Due to anomalies in the shape of the Earth and to the asymmetry of the matter density distribution inside the Earth, the Earth gravity potential cannot be expressed as a simple an-

alytical form. The Earth gravity field is usually approximated by a spherical harmonics series, and the set of all the gravitational potential coefficients in an infinite series expansion of spherical harmonics represents the Earth gravity field model.

The idea that the Earth gravity potential can be expressed as an infinite series of spherical harmonics has been widely used in geoscience research, and it is a basic method in Earth sciences and gravity satellite research. The literature contains conclusions about the relationships between disturbing potential coefficients and matter density anomalies inside the Earth [Jian 1994]. It was believed that lower degree potential coefficients reflect deep Earth matter density anomalies, while higher degree potential coefficients reflect shallow Earth matter density anomalies. By using the GRACE time-varying gravity-field model, global water storage changes were analyzed in Xuhua et al. [2006], Antarctic ice-sheet mass changes were studied in Guangbin et al. [2009], and application of a gravity-field model in tectonic detection was analyzed in Leyang et al. [2007]. At the same time, the spherical harmonics infinite series expansion of the Earth gravitational potential has been widely used in satellite gravity measurements. Satellites can measure the Earth gravity field, such as CHAMP, GRACE and GOCE, which were designed for recovering gravity potential coefficients in special bands. Among these three satellites, CHAMP has measured the Earth gravity field using orbit perturbation theory, which has helped to detect lower degree potential coefficients [Reigber et al. 2003]. GRACE measured the Earth gravity field by satellite-to-satellite tracking in a low Earth orbit, which helped in the detection of the lower- and middle-degree potential coefficients [Reigber et al. 2005, Zhao et al. 2011]. GOCE has used gravity gradient measurements that have helped to detect middle- and higher-degree potential coefficients [Muzi and Allasio 2003].

In the Earth gravity field model, gravitational potential coefficients are projections of gravitational potential on the

corresponding spherical harmonics by degree and order in the whole space, and they reflect the spectral composition of the gravitational potential in the whole space. However, gravitational potential coefficients cannot reflect the spectral composition of gravitational potential in a local space, which is a shortcoming of conventional Earth gravity-field models. Although spherical cap harmonic analysis (SCHA) can give the spectral composition of gravitational potential on a spherical cap [De Santis et al. 1999], because of less gravity potential coefficients, the spectral structure of the spherical cap area reflected by a SCHA model is limited. In the present study, based on the results in Slepian and Pollak [1961], the Earth gravitational potential was projected onto spherical harmonic functions in a local area, and by appropriate mathematical expressions, the signal-strength model for the gravity potential spectral component in a local space was established. This model will be helpful for Earth-science research and gravity satellite measurements.

## 2. A signal-strength model for gravity-field spectrum components in a local space

We establish a spherical coordinate system with the center of the Earth as the origin, and we take the $z$-axis and the Earth rotation axis in the same direction, as is shown in Figure 1. The spherical harmonic expansion of Earth's gravitational potential is:

$$V(\rho,\theta,\lambda) = \tag{1}$$
$$\frac{GM}{\rho}\left[1 + \sum_{n=2}^{\infty}\sum_{k=0}^{n}\left[\frac{a}{\rho}\right]^{n}(\overline{C}_{nk}\cos k\lambda + \overline{S}_{nk}\sin k\lambda)\overline{P}_{nk}(\cos\theta)\right],$$

where the definition of the spherical coordinates $(\rho,\theta,\lambda)$ is shown in Figure 1, and $G$ is the gravitational constant, $M$ is the Earth mass, $a$ is the semi-major axis of the Earth ellipsoid, $\{\overline{C}_{nk},\overline{S}_{nk}\}$ are the gravitational potential coefficients, and $\overline{P}_{nk}(\cos\theta)$ is the fully normalized associated Legendre polynomial. The relationship between $\overline{P}_{nk}(\cos\theta)$ and the associated Legendre polynomial, $P_{nk}(\cos\theta)$, is:

$$\overline{P}_{nk}(\cos\theta) = \tag{2}$$
$$\sqrt{(2n+1)\frac{2}{\delta_k}\frac{(n-k)!}{(n+k)!}}P_{nk}(\cos\theta), \quad \delta_k = \begin{cases} 2, k=0 \\ 1, k\neq 0 \end{cases}.$$

The nonspherical Earth perturbation potential function can be given from Equation (1):

$$R(\rho,\theta,\lambda) = \tag{3}$$
$$\frac{GM}{\rho}\sum_{n=2}^{\infty}\sum_{k=0}^{n}\left[\frac{a}{\rho}\right]^{n}(\overline{C}_{nk}\cos k\lambda + \overline{S}_{nk}\sin k\lambda)\overline{P}_{nk}(\cos\theta).$$

By the orthogonality of spherical harmonics functions, the gravitational potential coefficients $\{\overline{C}_{nk},\overline{S}_{nk}\}$ can be derived as:
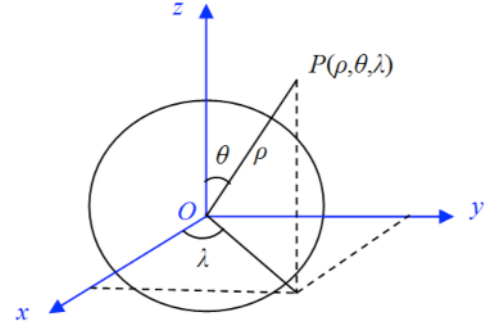


**Figure 1.** Spherical coordinate system with the Earth center as its origin.

$$\overline{C}_{nk} = \frac{1}{2\sqrt{2}\pi}\frac{\rho}{GM}\left[\frac{\rho}{a}\right]^{n}\sqrt{\frac{2n+1}{\delta_k}\frac{(n-k)!}{(n+k)!}} \tag{4}$$
$$\iint_{\Omega}R(\rho,\theta,\lambda)P_{nk}(\cos\theta)\sin\theta \cos k\lambda d\theta d\lambda,$$

$$\overline{S}_{nk} = \frac{1}{2\sqrt{2}\pi}\frac{\rho}{GM}\left[\frac{\rho}{a}\right]^{n}\sqrt{\frac{(2n+1)(n-k)!}{(n+k)!}} \tag{5}$$
$$\iint_{\Omega}R(\rho,\theta,\lambda)P_{nk}(\cos\theta)\sin\theta \sin k\lambda d\theta d\lambda,$$

where $\Omega$, the whole spherical surface, is the integral area. $\Omega$ can be divided into $n$ parts,

$$\Omega = \{\Omega_1 \quad \Omega_2 \quad ... \quad \Omega_n\}, \tag{6}$$

where, $\Omega_i$ ($i$=1,2,...,$n$) are the local areas on the spherical surface, as shown in Figure 2. $\Omega_i$ can be described by a certain longitude and latitude range, and its center is of interest.

In Equations (4) and (5), if the integral area $\Omega$ is changed into $\Omega_i$, then projections of the nonspherical Earth perturbation potential $R(\rho,\theta,\lambda)$ on $n$-degree and $k$-monics in the local area $\Omega_i$ can be obtained:

$$\overline{C}_{nk,i} = \frac{1}{2\sqrt{2}\pi}\frac{\rho}{GM}\left[\frac{\rho}{a}\right]^{n}\sqrt{\frac{2n+1}{\delta_k}\frac{(n-k)!}{(n+k)!}} \tag{7}$$
$$\iint_{\Omega_i}R(\rho,\theta,\lambda)P_{nk}(\cos\theta)\sin\theta \cos k\lambda d\theta d\lambda,$$

$$\overline{S}_{nk,i} = \frac{1}{2\sqrt{2}\pi}\frac{\rho}{GM}\left[\frac{\rho}{a}\right]^{n}\sqrt{\frac{(2n+1)(n-k)!}{(n+k)!}} \tag{8}$$
$$\iint_{\Omega_i}R(\rho,\theta,\lambda)P_{nk}(\cos\theta)\sin\theta \sin k\lambda d\theta d\lambda.$$

Then,
$$\overline{C}_{nk} = \sum_{i=1}^{n}\overline{C}_{nk,i}, \quad \overline{S}_{nk} = \sum_{i=1}^{n}\overline{S}_{nk,i}. \tag{9}$$

It is known that $\{\overline{C}_{nk,i},\overline{S}_{nk,i}\}$ reflect projections of the nonspherical Earth perturbation potential on $n$-degree and $k$-order spherical harmonics $\{P_{nk}(\cos\theta)\cos k\lambda, P_{nk}(\cos\theta)\sin k\lambda\}$ in the local areas $\Omega_i$, which represent the signal strengths of $n$-degree and $k$-order spherical harmonic components in $\Omega_i$, while $\{\overline{C}_{nk},\overline{S}_{nk}\}$ reflect the sum of these projections in the
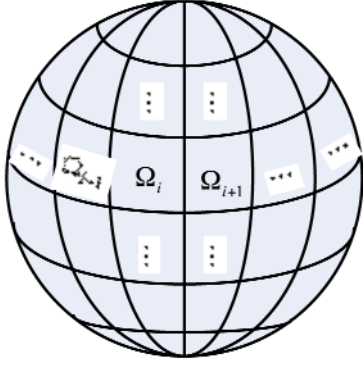
**Figure 2.** Sketch map of the local region $\Omega_i$ on the spherical surface.

whole area $\Omega$, and represent the total signal strength of $n$-degree and $k$-order spherical harmonic components in the whole area. For purposes of satellite gravity field measurements, if the recovery frequency bands involved contain $n$-degree potential coefficient, sampling data at the places where the signal of the $n$-degree spectral component is stronger helps to increase the signal-to-noise ratio of $n$-degree spectrum components and increase the recovery accuracy of $n$-degree potential coefficients.

The signal strength of $n$-degree and $k$-order spectrum component in the local areas $\Omega_i$ can be computed by Equations (7) and (8), which is approximately equivalent to the computing of the data with perturbation potentials in Equations (4) and (5), multiplied by a window function. The window function takes the maximum in $\Omega_i$, and the farther the distance away from $\Omega_i$ it is, the smaller the window function will be. Here, on the sphere surface of fixed radius $\rho_0$, the signal strength of $n$-degree and $k$-order spectrum components in the local area $\Omega_0$ will be computed, where the center of $\Omega_0$ is $(\rho_0, \theta_0, \lambda_0)$.

The unit vector from the sphere center to the point $(\rho_0, \theta_0, \lambda_0)$ is:

$$\vec{e}_0 = (\sin\theta_0 \cos\lambda_0 \quad \sin\theta_0 \sin\lambda_0 \quad \cos\theta_0). \quad (10)$$

The unit vector from the sphere center to any point, $(\rho_0, \theta, \lambda)$, on the sphere surface is:

$$\vec{e} = (\sin\theta \cos\lambda \quad \sin\theta \sin\lambda \quad \cos\theta). \quad (11)$$

Assuming that the angle between two unit vectors in the above is $\psi$, then:

$$\cos\psi = \vec{e}_0 \cdot \vec{e} = \sin\theta \sin\theta_0 \cos(\lambda - \lambda_0) + \cos\theta \cos\theta_0 . \quad (12)$$

Thus,

$$\psi = \text{arc} \cos[\sin\theta \sin\theta_0 \cos(\lambda - \lambda_0) + \cos\theta \cos\theta_0]. \quad (13)$$

On the sphere surface of radius $\rho_0$, making a window function with the point $(\theta_0, \lambda_0)$ as its center,

$$H_{\theta_0, \lambda_0}(\theta, \lambda) = e^{-\xi\psi^2} . \quad (14)$$

As $\psi$ is the spherical distance from $(\rho_0, \theta, \lambda)$ to $(\rho_0, \theta_0, \lambda_0)$, the window function satisfies $0 < H \leq 1$. The window function is 0 only for the point $(\theta_0, \lambda_0)$, and the longer the spherical distance from $(\theta, \lambda)$ to $(\theta_0, \lambda_0)$ is, the smaller the $H$ is. The attenuation factor satisfies $\xi > 0$. The greater $\xi$ is, the narrower $H$ is, and the smaller $\xi$ is, the wider $H$ is.

Multiplying Equations (4) and (5) by the window function in Equation (14) and substituting Equation (3) gets the sine and cosine signal strength of $n$-degree and $k$-order spectrum components in the local area $\Omega_0$ where the center is $(\rho_0, \theta_0, \lambda_0)$,

$$\overline{C}_{nk}{}^* = \frac{1}{2\sqrt{2}\,\pi}\left[\frac{\rho}{a}\right]^n \sqrt{\frac{2n+1}{\delta_k}\frac{(n-k)!}{(n+k)!}} \sum_{l=2}^{\infty} \sum_{m=0}^{l} \left[\frac{a}{\rho}\right]^l \quad (15)$$
$$\iint_{\Omega} H_{\theta_0, \lambda_0}(\theta, \lambda)(\overline{C}_{lm}\cos k\lambda + \overline{S}_{lm}\sin k\lambda)$$
$$\overline{P}_{lm}(\cos\theta)P_{nk}(\cos\theta)\sin\theta \, \cos k\lambda \mathrm{d}\theta \mathrm{d}\lambda$$

$$\overline{S}_{nk}{}^* = \frac{1}{2\sqrt{2}\,\pi}\left[\frac{\rho}{a}\right]^n \sqrt{\frac{(2n+1)(n-k)!}{(n+k)!}} \sum_{l=2}^{\infty} \sum_{m=0}^{l} \left[\frac{a}{\rho}\right]^l \quad (16)$$
$$\iint_{\Omega} H_{\theta_0, \lambda_0}(\theta, \lambda)(\overline{C}_{lm}\cos k\lambda + \overline{S}_{lm}\sin k\lambda)$$
$$\overline{P}_{lm}(\cos\theta)P_{nk}(\cos\theta)\sin\theta \, \sin k\lambda \mathrm{d}\theta \mathrm{d}\lambda.$$

Then the signal strength of $n$-degree and $k$-order spectrum components in the local area $\Omega_0$ is:

$$E_{nk} = \sqrt{(\overline{C}_{nk}{}^*)^2 + (\overline{S}_{nk}{}^*)^2} . \quad (17)$$

## 3. Comparison among spherical harmonic analysis, spherical cap harmonic analysis, and translated origin spherical cap harmonic analysis

From spherical harmonics expansion, it is known that the gravitational potential can be seen as the superposition of an infinite number of spherical harmonic waves, and potential coefficients are just the vibration amplitudes of these spherical harmonic waves, which reflect the energy of corresponding spherical harmonic waves. By projecting gravitational potential on spherical harmonic functions in the global area, i.e., using spherical harmonic analysis (SHA), a conventional gravity model can be obtained, and one potential coefficient reflects the total energy of the corresponding spherical harmonic in the global area. For the projection of gravitational potential on spherical harmonic functions in a local area, i.e., the method investigated here, we get the energy of the spherical harmonics in the local area. This is the relationship between SHA and our method.

Spherical cap harmonic analysis (SCHA) is a method for the gravitational potential on the spherical cap, which was first proposed by Haines, and the effectiveness of this method has been shown by geomagnetic field modeling [Haines 1985]. SCHA was first applied in geodesy by Jiancheng, with an SCHA model for a local gravity field given
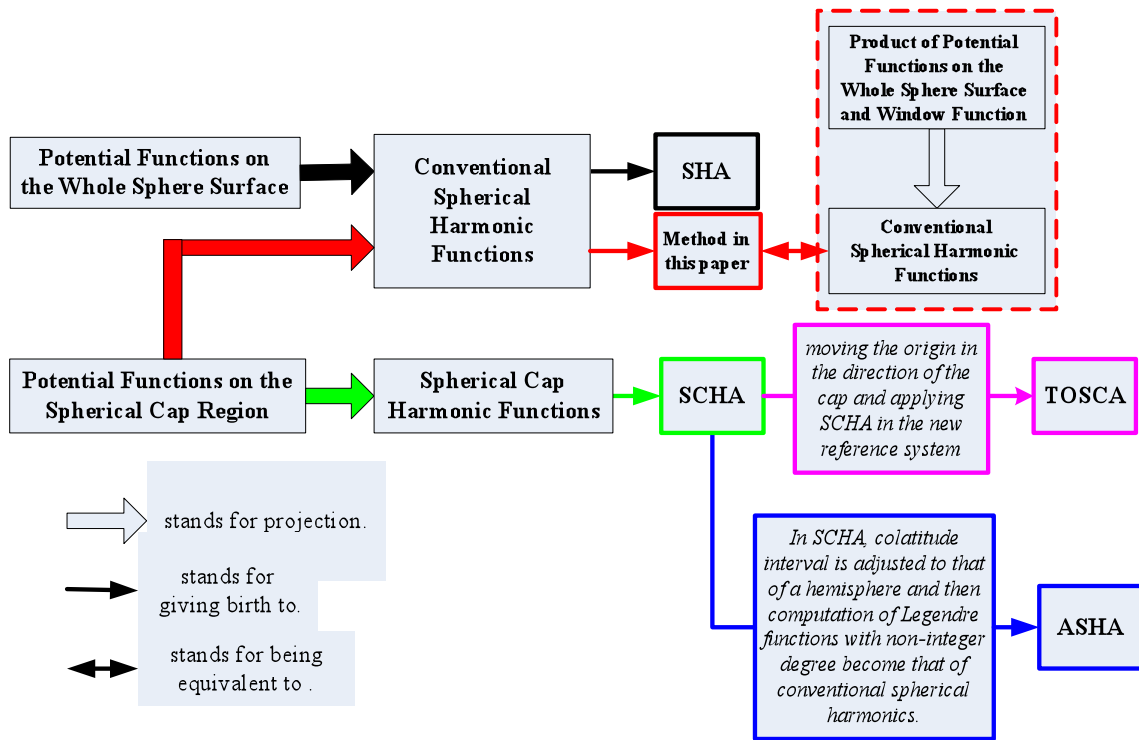
**Figure 3.** The relationships between SHA, SCHA, TOSCA, ASHA and the method in the present study.

[Jiancheng et al. 1995, De Santis and Torta 1997]. The basic functions in SCHA are composed of noninteger degree associated Legendre polynomials and trigonometric functions, with orthogonality and completeness, and they can approximate the Earth gravitational potential function on the spherical cap. The nonspherical perturbation potential on the spherical cap can be expressed as:

$$R_\Omega(\rho, \theta, \lambda) = \qquad\qquad (18)$$

$$\frac{GM}{\rho} \sum_{k=2}^{\infty} \sum_{m=0}^{k} \left[\frac{a}{\rho}\right]^{n_k} (C_{km} \cos m\lambda + S_{km} \sin m\lambda) P_{n_k m}(\cos\theta),$$

where $P_{n_k m}(\cos\theta)$ is the noninteger degree associated Legendre polynomial. From a mathematical point of view, SCHA is the method that the potential on a spherical cap is projected on spherical cap harmonic functions. Compared to the SHA model, when the same spatial resolution for a local gravity field is achieved, fewer gravitational potential coefficients are required in the SCHA model [Fuqing and Jinhai 2000], which means that the SCHA model contains less spectrum components than SHA model. At the same time, with SCHA, the nonorthogonality of odd basis functions ($k$-$m$ = odd) and even basis functions ($k$-$m$ = even) can lead to computation instability of potential coefficients and deterioration in the SCHA model at the edge of the cap when the data distribution is not uniform over the region [De Santis 1991].

For the computation instability of potential coefficients in SCHA, De Santis [1991] proposed translated origin spherical cap harmonic analysis (TOSCA), which was mathematically constructed by moving the new origin in the direction of the cap region and applying SCHA in the new reference sys-

tem. TOSCA can greatly improve the detail in the central regions and can smooth the observations at the edge of the cap. In addition, for the computation of more complex Legendre functions with non integer harmonic degrees in SCHA, De Santis proposed adjusted SHA (ASHA), in which the co-latitude interval was adjusted to a hemisphere, and then conventional spherical harmonics could be used [De Santis 1992].

Just like SCHA and TOSCA, the method in the present study can be used for analysis of a potential spectrum in a local area. However, in our method, the gravitational potential in a local area is directly projected on the spherical harmonic functions, not on the spherical cap harmonic functions, which compared to SCHA, can obtain more potential coefficients and consequently a more comprehensive spectrum structure for the local area, although the computation cost will increase. To facilitate the mathematical expressions, the product of gravitational potential and an exponential function called the window function, which decreases with distance from the center of the local area involved, is projected on the spherical harmonic functions in the global region, which indirectly obtains the projection of the gravitational potential in the local region; i.e., Equations (15) and (16). It is in the global region for the projection of gravitational potential that the observation data scope increases and the detail in the central regions is greatly improved, which is similar to De Santis 1991, and helps to reduce errors. In De Santis [1991], the details in the central regions were greatly improved by using more observation data under a new coordinate system that was obtained by moving the origin of the old coordinates upwards from the center of the Earth.

The relationships between SHA, SCHA, TOSCA and ASHA and the method in the present study are shown in Figure 3.
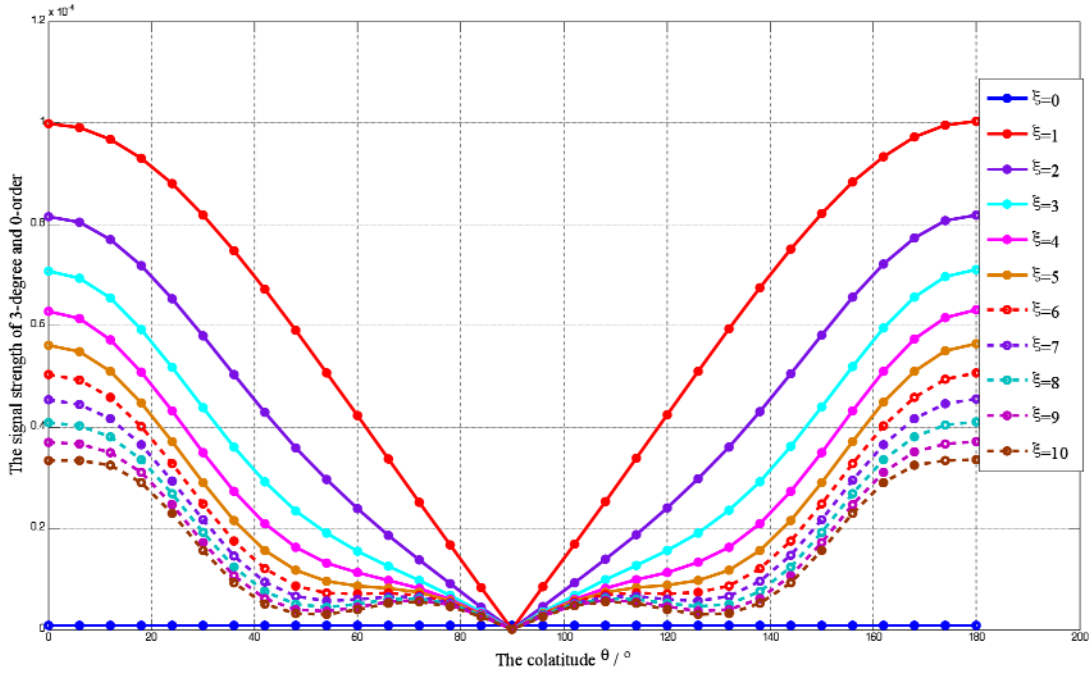
**Figure 4.** The signal strength of third-degree and zero-order spherical harmonics at different co-latitudes (longitude, $\lambda = \pi/4$).
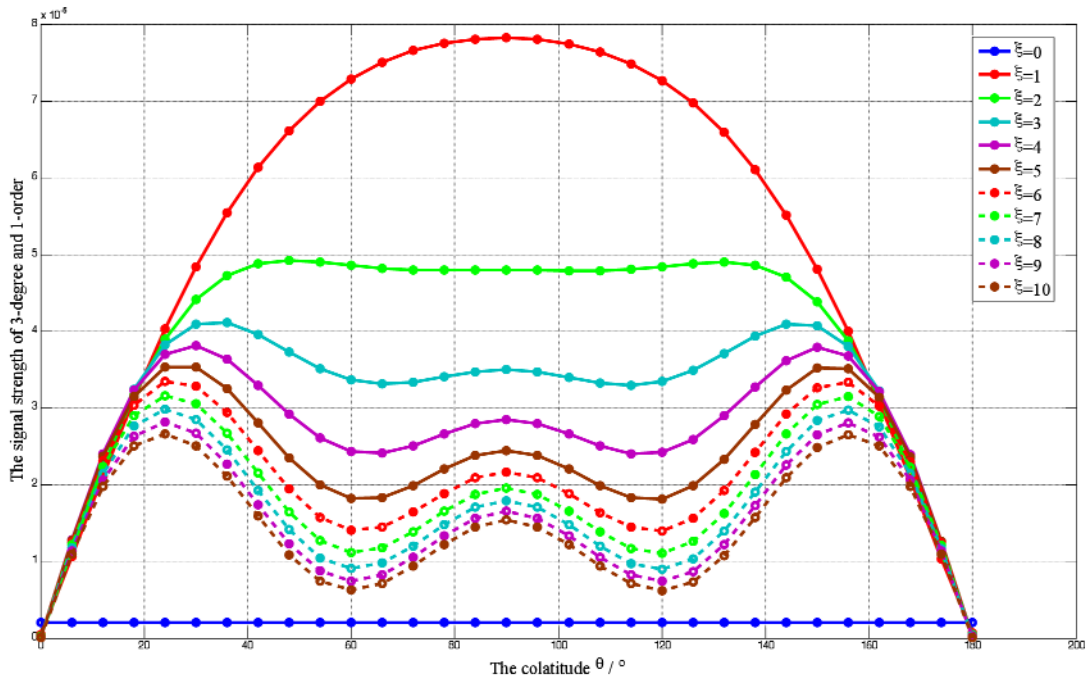


**Figure 5.** The signal strength of third-degree and first-order spherical harmonics at different co-latitudes (longitude, $\lambda = \pi/4$).

## 4 Numerical computations

Take the first 10 degrees in the Earth Gravitational Model 1996 (EGM96) as a simulation of the Earth gravity field. The attenuation factor $\xi$ determines the size of local area selected, and a right attenuation factor can be obtained by computational results. According to Equations (15), (16) and (17), in the case of $\xi = 0 \sim 10$, the computed signal strength of the third-degree potential coefficient along the longitude $\lambda = \pi/4$ at the altitude of 200 km is shown in Figures 4-7.

From Figures 4-7, it is known that:

(1) When attenuation factor $\xi = 0$, the signal strength of each spherical harmonic component does not change with the co-latitudes. The reason for this is that $\xi = 0$ means the local area is just the entire spherical surface, and their projections on spherical harmonics are certainly the same, making the signal strength of each spherical harmonic component equal in any area of the spherical surface.

(2) With the increase in the attenuation factor, local features gradually appear in the signal strength of each spherical harmonic component. With different attenuation factors, the sizes of selected local areas are different, and consequently there will be some differences among the signal strengths of each spherical harmonic component, although their tendencies with the co-latitudes are consistent.
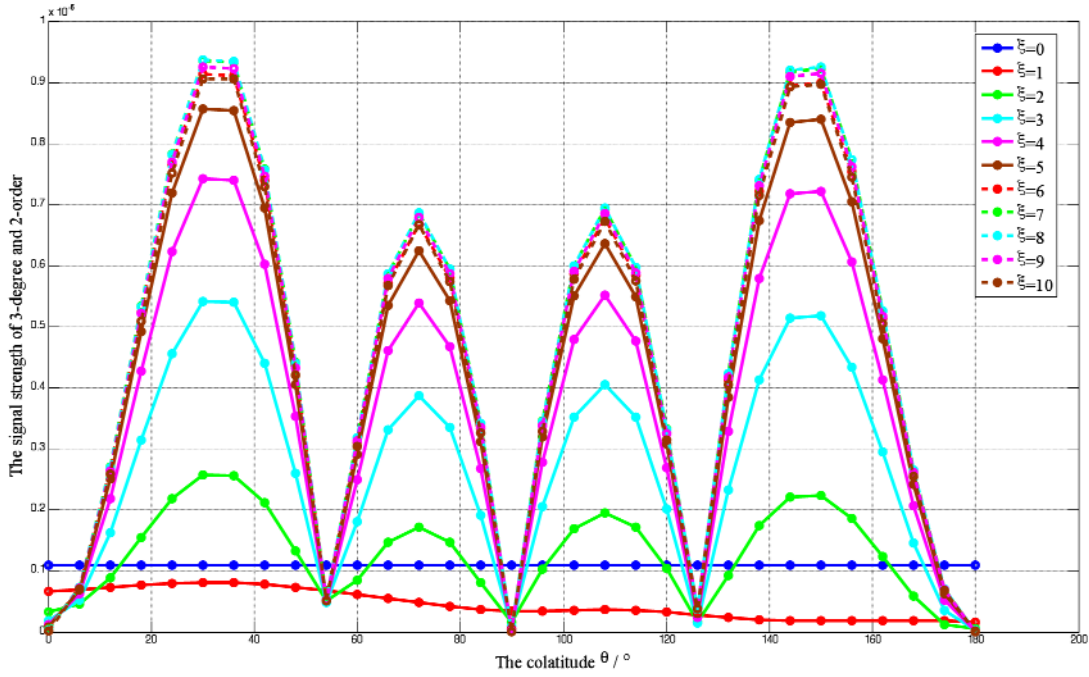
**Figure 6.** The signal strength of third-degree and second-order spherical harmonics at different co-latitudes (longitude, $\lambda = \pi/4$).
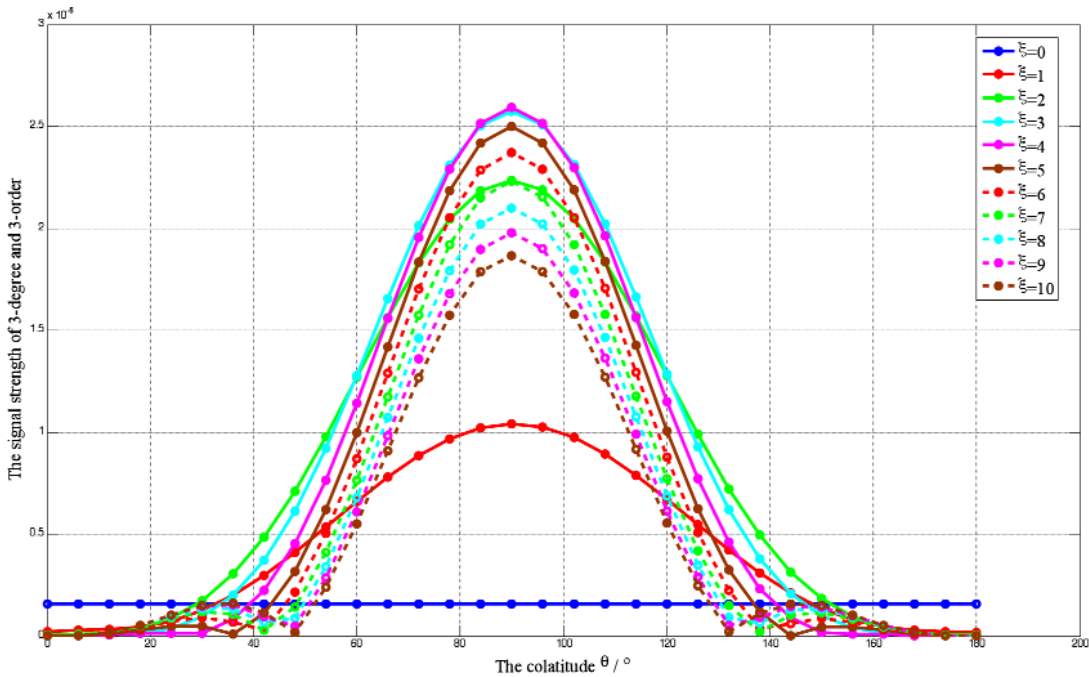


**Figure 7.** The signal strength of third-degree and third-order spherical harmonics at different co-latitudes (longitude, $\lambda = \pi/4$).

According to Figures 4-7, when $\xi = 5$, the change tendency for the signal strength of each spherical harmonic component with co-latitudes can be shown clearly. Take the attenuation factor of the window function as 5, as shown in Figure 8, and analyze the distribution law for the signal strength of the third-degree spherical harmonic component along the whole sphere surface.

From Equations (15), (16) and (17), the signal strength distributions of the third-degree potential coefficients on the sphere surface at the altitude of 200 km are shown in Figures 9 to 12.

Figures 9 to 12 show that the signal strength distributions of the third-degree potential coefficients on the sphere surface are independent of the longitude. The zero-order, first-order and second-order components are stronger near the two poles of the Earth, and weaker near the equator, while the third-order is weaker near the two poles and stronger near the equator.

From Equation (3), it is known that when the longitude $\lambda$ is unchanged, the associated Legendre polynomial, $P_{nk}(\cos\theta)$, reflects the change tendency of the $n$-degree and $k$-order spherical harmonic with the co-latitude. This represents the signal strength change tendency of $n$-degree spherical harmonics in the conventional gravity model, such as the EGM96
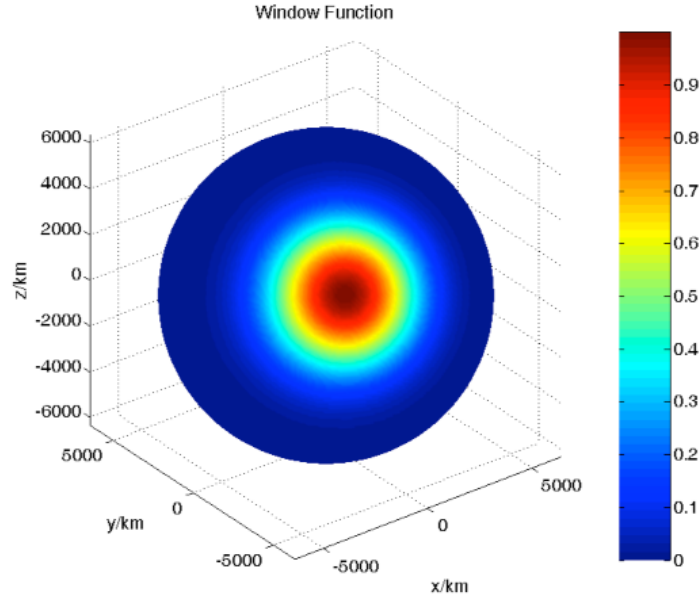
**Figure 8.** The window function with an attenuation factor $\xi = 5$ on the Earth surface.
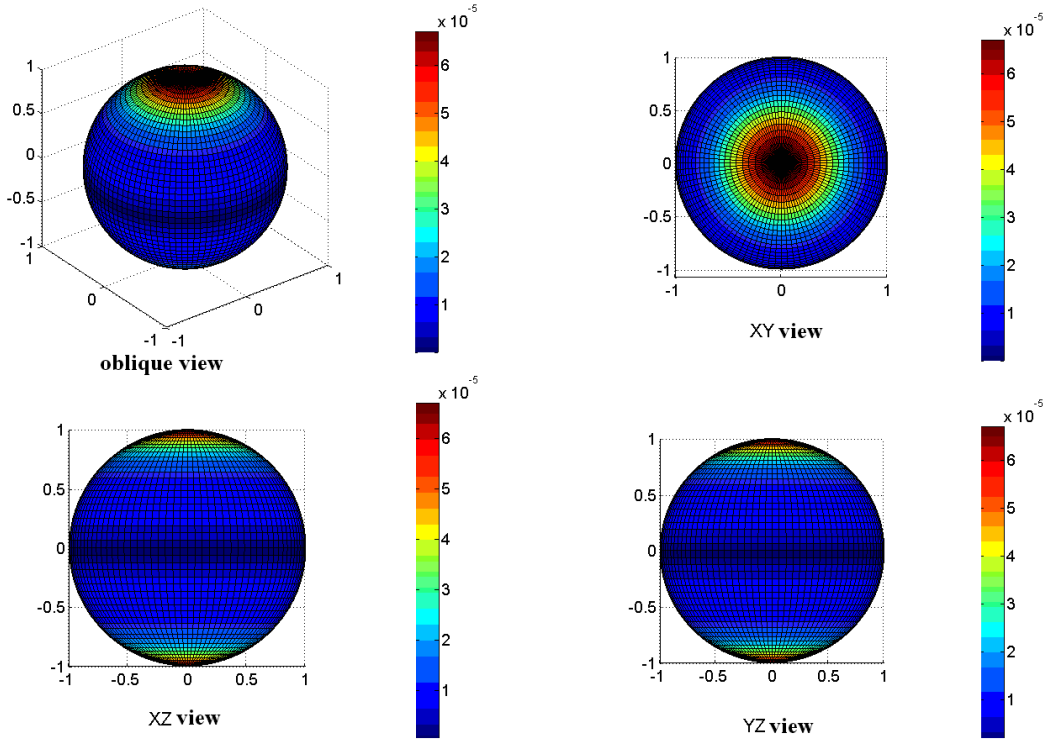


**Figure 9.** The distribution of $\sqrt{\overline{C}_{30}^{*\,2} + \overline{S}_{30}^{*\,2}}$ on the sphere surface.

model. Figure 13 shows the changes of $P_{30}(\cos\theta)$, $P_{31}(\cos\theta)$, $P_{32}(\cos\theta)$ and $P_{33}(\cos\theta)$ with the co-latitudes, and Figure 14 shows the signal strengths of third-degree spherical harmonic components along the longitude $\lambda = \pi/4$, with attenuation factor $\xi = 5$. From the comparison of Figures 13 and 14, it is known that for the change tendency of first-order and third-order spherical harmonic components with the co-latitudes, the results given by the EGM96 model and the method in the present study are the same, while for the zero-order and third-order, the results from the EGM96 model and the present method are different. This shows that the method in the present study can give

a more sophisticated structure for the gravitational potential, and increases the information describing the Earth gravity field, which cannot be seen from the conventional gravity model.

## 5. Conclusions

Here, by projecting the Earth gravitational potential on the spherical harmonics in a local area, the signal strength model for each spectral component in the Earth gravity field model in a local area was established. Compared to the traditional Earth gravity-field model, i.e., SHA model, this can provide a more sophisticated gravity field spectrum structure in
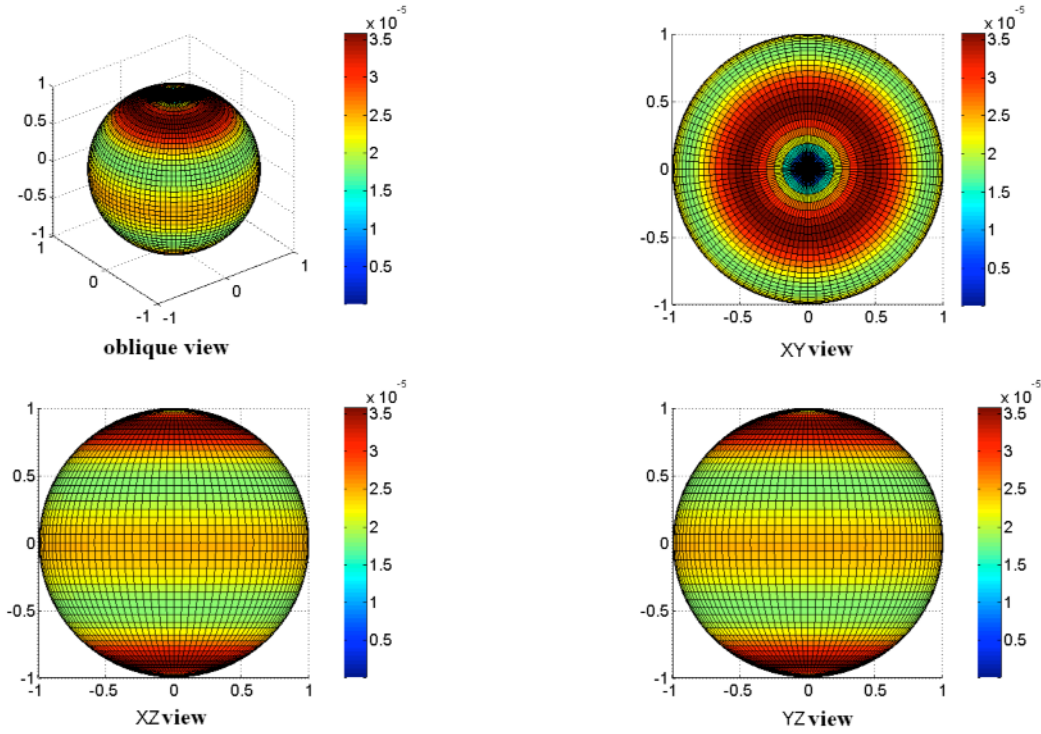
**Figure 10.** The distribution of $\sqrt{\overline{C}_{31}^{*\,2} + \overline{S}_{31}^{*\,2}}$ on the sphere surface.



**Figure 11.** The distribution of $\sqrt{\overline{C}_{32}^{*\,2} + \overline{S}_{32}^{*\,2}}$ on the sphere surface.

the local area and increase the information that describes the Earth gravity field, which cannot be seen from the conventional gravity model. Compared to SCHA, the present model can reflect more spectral components in the local area, which helps to design a more reasonable satellite orbit and sampling area for the given gravity field measurement band, and thus we can strengthen the gravity satellite sample data at the places where the signal of the potential coefficients is stronger,

and improves the accuracy of the gravity field measurement.

In the end, the signal strength distributions for third-degree coefficients were computed. These results show that the signal strength distributions of third-degree coefficients are independent of the longitude, and the zero-order, first-order and second-order coefficients have stronger signals nearer the two poles of the Earth, while the third-order coefficient has a stronger signal near the equator.
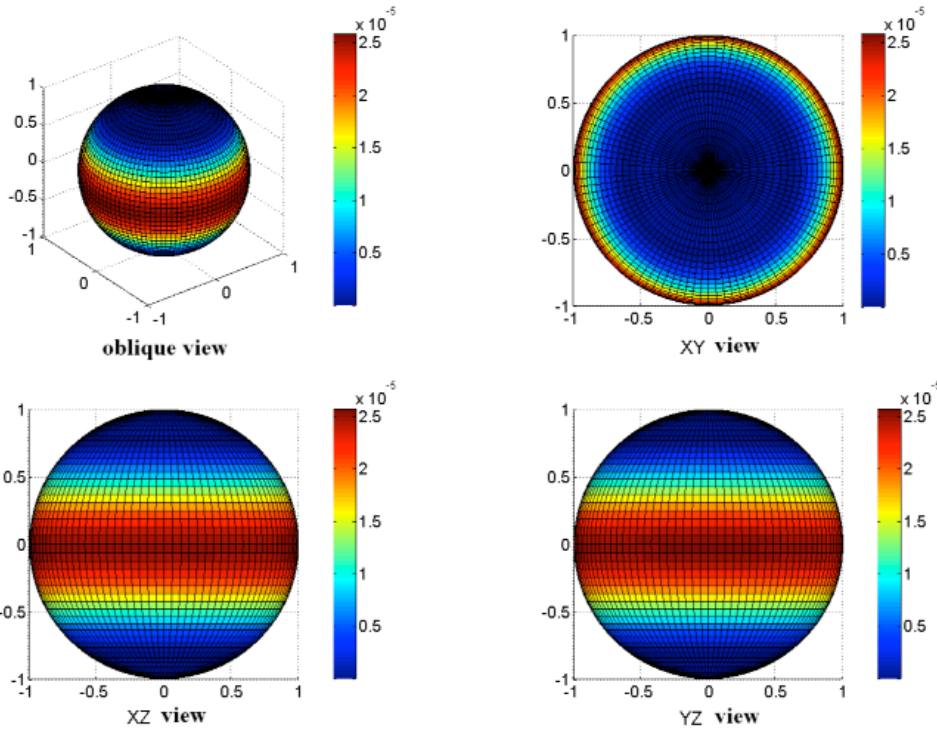
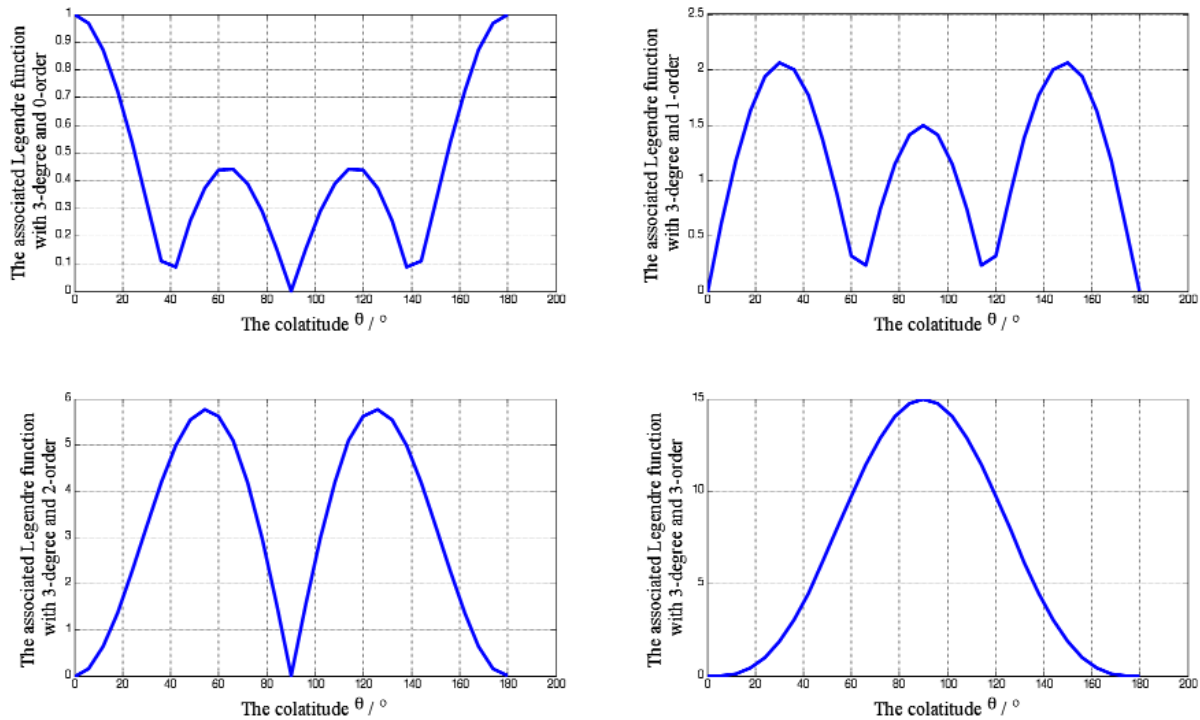**Figure 12.** The distribution of $\sqrt{\overline{C}_{33}^{*\,2} + \overline{S}_{33}^{*\,2}}$ on the sphere surface.



**Figure 13.** The associated Legendre polynomials $P_{30}(\cos\theta)$, $P_{31}(\cos\theta)$, $P_{32}(\cos\theta)$ and $P_{33}(\cos\theta)$.

## References

De Santis, A. (1991). Translated origin spherical cap harmonic analysis, Geophysical Journal International, 106, 253-263

De Santis, A. (1992). Conventional spherical harmonic analysis for regional modeling of the geomagnetic field, Geophysical Research Letters, 19 (10), 1065-1067.

De Santis, A., and J.M. Torta (1997). Spherical cap harmonic analysis: a comment on its proper use for local gravity field representation, Journal of Geodesy, 71, 526-532.

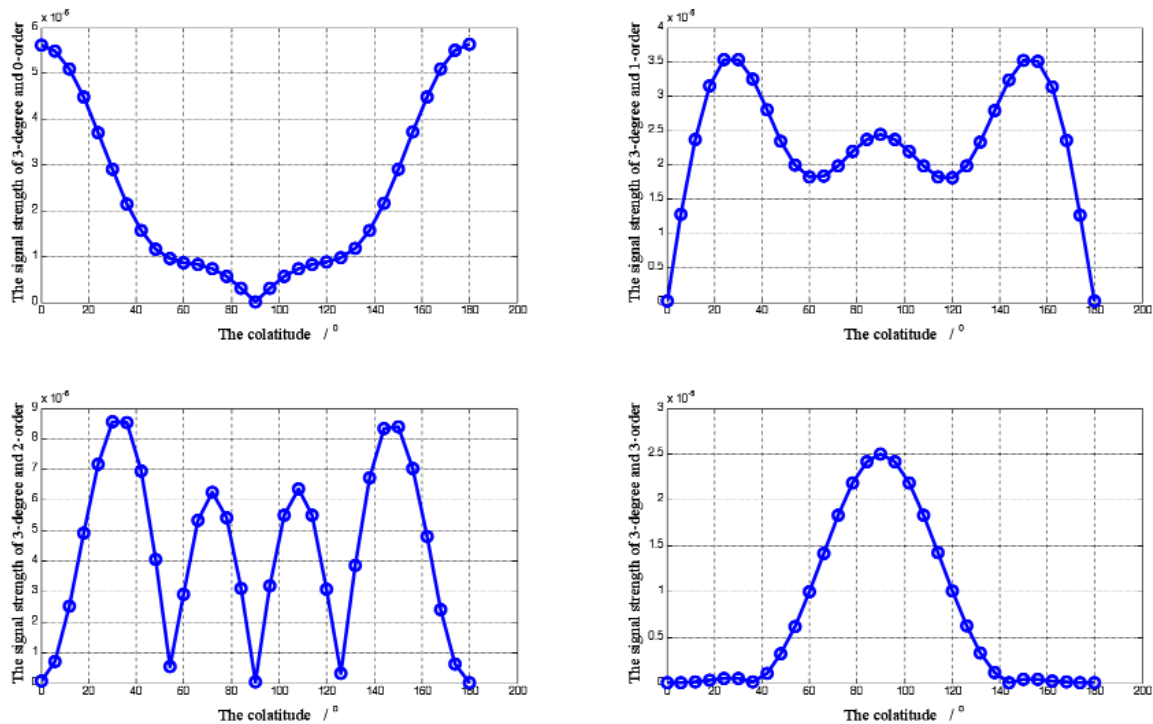De Santis, A., J.M. Torta and F.J. Lowes (1999). Spherical cap

**Figure 14.** The signal strength of third-degree spherical harmonics at different co-latitudes (longitude, $\lambda = \pi/4$).

harmonics revisited and their relationship to ordinary spherical harmonics, Phys. Chem. Earth (A), 24 (11-12), 935-941.

Fuqing, P., and Y. Jinhai (2000). The characters and computation of Legendre function with non-integral degree in SCHA, Acta Geodaetica et Cartographica Sinica, 29 (3), 204-208 (in Chinese).

Guangbin, Z., L. Jiancheng, W. Hanjiang, W. Zhengtao (2009). Investigation on the mass variations of ice sheet in Antarctic with GRACE time-variable gravity models, Geomatics and Information Science of Wuhan University, 34 (10), 1185-1189 (in Chinese).

Haines, G.V. (1985). Spherical cap harmonic analysis, J Geophys Res, 90, 2583-2591.

Jian, F. (1994). Investigation of anomaly density by using satellite gravity data, Progress in Geophysics, 3, 60-65 (in Chinese).

Jiancheng, L., C. Dingbo and N. Jinsheng (1995). Spherical cap harmonic expansion for local gravity field representation, Manuscr. Geod., 20, 265-277.

Jinsheng, N. (2001). Following the developments of the world, devoting to the study on the Earth gravity field, Geomatics and Information Science of Wuhan University, 26 (6), 471-474 (in Chinese).

Jinsheng, N. (2002). The satellite gravity gravity surveying technology and research of Earth's gravity field, Journal of geodesy and geodynamics, 22 (1), 1-5 (in Chinese).

Leyang, W., Z. Jianjun and Z. Ziqiang (2007). Applicable study of EIGEN-GRACE02S gravity model on detection of Earth's crust tectonics, Journal of geodesy and geodynamics, 27, 31-34 (in Chinese).

Muzi, D., and A. Allasio (2003). GOCE: the first core Earth explorer of ESA's Earth observation programme, Acta Astronautica, 54, 167-175.

Reigber, Ch., P. Schwintzer, K.H. Neumayer, F. Barthelmes, R. König, Ch. Förste, G. Balmino, R. Biancale, J.M. Lemoine, S. Loyer, S. Bruinsma, F. Perosanz and T. Fayard (2003). The CHAMP-only Earth gravity field model EIGEN-2, Advances in Space Research, 31 (8), 1883-1888.

Reigber, Ch., R. Schmidt, F. Flechtner, R. König, U. Meyer, K.-H. Neumayer, P. Schwintzer and S.Y. Zhu (2005). An Earth gravity field model complete to degree and order 150 from GRACE: EIGEN-GRACE02S, Journal of Geodynamics, 39, 1-10.

Slepian, D., and H.O. Pollak (1961). Prolate spheroidal wave functions, Fourier analysis and uncertainty — I, The Bell System Technical Journal, 40, 43-64.

Xiaoguang, H., X. Houze and L. Dajie (2000). Earth's density flat rate and the hypothesis of latitudinal normal density, Science in China (Series D), 30 (4), 436-441 (in Chinese).

Xuhua, Z., W. Bin, P. Bibo, X. Houze (2006). Detection of global water storage variation using GRACE, Chinese J . Geophys., 49 (6), 1644-1650 (in Chinese).

Zhao, Q., J. Guo, Z. Hu, Ch. Shi, J. Liu, H. Cai and X. Liu (2011). GRACE gravity field modeling with an investigation on correlation between nuisance parameters and gravity field coefficients, Advances in Space Research, 47, 1833-1850.

*Corresponding author: Liu Hongwei,
Institute of Aerospace Science and Engineering, National University of Defence Technology, Changsha, China; email: liuhw05@163.com.